Aircraft tire temperature at touchdown with wheel prerotation

Article (Accepted Version)

Aircraft Tire Temperature at Touchdown with Wheel Pre-rotation

Abdurrhman A. Alroqi[1] and Weiji Wang[2]
University of Sussex, Brighton, UK, BN1 9QT

Yong Zhao[3]
Alfaisal University, Al Maathar Road, P.O. Box 50927, Riyadh 11533, KSA

Because of the skidding process that occurs when a heavy aircraft's main landing gear tires touchdown, since the 1940s, a number of ideas have been patented to improve tire safety and decrease the substantial wear and smoke during every landing by spinning the gear wheels before touchdown. In this paper, a coupled structural – thermal transient analysis in ANSYS has been used to model a single wheel main landing gear as a mass-spring system. This model has been chosen to analyze the wheel's dynamic behavior and tire tread temperature during the short period from static to a matching free-rolling velocity in which the wheel is forced to accelerate by the friction between the tire and ground. The tire contact surface temperature has been calculated for both the initially static and pre-spun wheels in order to compare the temperature levels for different initial rotations and to validate the use of pre-spinning technique.

Nomenclature

F_x = longitudinal friction force reacted on tire contact patch (N)

F_y = downward force reacted by the landing gear structure (N)

F_R = reaction force reacted at tire contact patch (N)

m, m_w = weight box and wheel mass respectively (kg)

c, c_t = shock absorber and tire damping coefficients respectively (Ns/m)

k, k_t = landing gear and tire linear stiffness respectively (N/m)

Y, δ = lumped mass vertical displacement and tire deflection respectively (m)

[1] PhD researcher, Department of Engineering and Design, aa-alroqi@hotmail.com.
[2] Senior Lecturer, Department of Engineering and Design, W.J.Wang@sussex.ac.uk.
[3] Chairman & Associate Professor of Mechanical Engineering, zyong@alfaisal.edu.

$\dot{y},\ \dot{\delta}$ = vehicle vertical velocity and tire deflection rates respectively (m/s)

$\ddot{\delta},\ \ddot{y}$ = tire deflection and vehicle vertical accelerations respectively (m/s^2)

μ = friction coefficient

v = aircraft's horizontal ground speed (m/s)

v_s = wheel skidding speed (m/s)

λ = wheel slip ratio

$R,\ r_e$ = free and effective wheel radiuses respectively (m)

$\dot{\omega}$ = wheel's acceleration (rad/s^2)

$C_{1,2,3,4}$ = runway surface types friction constants

I = wheel's moment of inertia, kg m^2

$\omega,\ \omega_i$ = wheel angular velocities after and prior to touchdown respectively (rad/sec)

q = heat generated by friction power ($\frac{W}{m^2}$)

k = thermal conductivity ($\frac{W}{m\ C^o}$), k_t for tire and k_r for runway

α = thermal diffusivity ($\frac{m^2}{s}$), α_t for tire and α_r for runway

ρ = material density ($\frac{Kg}{m^3}$)

c_v = material specific heat ($\frac{J}{Kg\ C^o}$)

T = tire tread temperature (C^o)

I. Introduction

THE approach speed of heavy aircraft to land is high, in order to maintain an acceptable sink rate, this leads to a great difference between the tangential velocity of the tire radius and the horizontal landing speed at touchdown. The tangent velocity of the tire is forced to accelerate so as to overcome the inertia of wheel/tire assembly to match the aircraft ground speed. The runway surface can only provide limited tangent friction between the tire and ground for the acceleration from static. Therefore, slip is inevitable. The slip normally takes place within a second and its distance ranges from several to dozens meters [1]. The heat generated by the slipping tire at touchdown is enough to melt a thin layer of tire tread rubber [2]. However, the majority of heat generated occurs when the wheel is at full skid [3]. The tire tread temperature rises

immediately during the tire skidding phase within 0.1 seconds to exceed the critical temperature [2]. Most of the tire tread material is natural rubber, which has the empirical formula $(C_5H_8)_n$ and its critical temperature is about 200^0C [2, 4]. Some experiments have shown that the rubber deposited on the concrete is at this temperature level [5]. At critical temperature, the bond linkages in the tread rubber material breaks and then wear occurs easily by abrasion force [2]. About one-third of rubber particles burn off under the skidding wheel is evaporates in the form of smoke, while the remaining proportion stays on the runway [6]. However, the rubber's contact temperature is a function of the force of friction and the skidding speed, and there is no way to avoid a high force of friction. [7]. Therefore, a reduction in the skidding speed in order to avoid a high slip ratio can be achieved by pre-spinning the wheels. This will allow for the avoidance of a high tread temperature and wear, a reduction in environmental pollution, and an increase in the number of tire cycles which is about 300 cycles (take-offs and landings) for heavy aircraft [8].

A. Aim of the Study

Patents have suggested that it is possible to spin the rear wheels before touchdown using wind turbines [9]. The wind energy generated by an approaching aircraft is at a high enough speed to be used by wind turbines to spin wheels. The wind energy will be at least equal to the speed of the aircraft. However, the wind turbine has limited efficiency, and to use it for aircraft, it should be small enough to fit in the aircraft undercarriage. It also is important to avoid extra weight or have any aerodynamic effects. In this paper, the model shows how much pre-rotation is sufficient in order to avoid rubber reaching its critical temperature without the need to fully spin wheels, which requires large wind turbines. A Boeing 747-400 single rear wheel has been modeled as a case study in this simulation. Only heat generation by work done has been investigated without strain energy, which is small when comparing it with friction power.

B. Literature Review

In the current literature, few studies have investigated the process by which the rubber of aircraft tires vaporizes during landing. Skid-marks are produced by material being detached by abrasion between slipping tires and the runway surface. In a previous study, we developed a Simulink model to estimate the reduction of aircraft tire wear that could be achieve by spinning the wheel before landing. We concluded that the 100% pre-rotated wheel lost just 1.07% of its tire material through abrasive wear compared to tire wear in a typical aircraft landing [10].

According to (Ref. [11]), the force of friction produced between the surfaces of the tire and runway is associated with the internal friction of the rubber, which is a bulk property. The gripping and sliding of rubber over a coarse surface

causes the friction to occur. These movements lead to energy loss, which can cause the tire to heat up enough so that smoke is produced.

In [12], the author developed a model allowing for the simulation of lateral "shimmy" oscillations in a Boeing 747-400 aircraft's main landing gear. Even though the extent of the research does not contain lateral dynamics, several important experimental data was recorded. For example, his research shows an experimental wheel-velocity time on a Boeing 747-400 aircraft during landing. This information is useful for validating simulations that investigate skidding time and distance. Measured data in both [12] and [13] demonstrate that tires accelerate from zero rotational speed to a free-rolling velocity within approximately 0.1 seconds from touchdown.

The authors in [14], developed an algorithm model to simulate and define aircraft tire wear and temperature during the use of an antilock braking system (ABS). They estimated the tread surface temperatures for different landing speeds in the range of 20 – 80 knots (10 – 41 m/s) and the total vehicle weight being 9979 kg. They used two methods: harmonic ABS cycling point wise and square wave on/off ABS braking point wise. However, the temperature they recorded reached 204 C^o within a portion of a second during maximum landing velocity.

In [15], the authors used a high speed linear tester (HiLiTe) at the Institute of Dynamics and Vibration Research in Hannover, Germany to investigate aircraft tire tread temperature while a wheel was at full skid ($\text{slip ratio} = 1$) at touchdown. They found that by using a block of rubber sliding on a concrete track for 5.5 m and a bellows cylinder to increase the vertical pressure being applied on the rubber, the sliding rubber temperature rose up from $22\ C^o$ to $171\ C^o$ after 2 m distance. This was effected by a $10\ \text{m/s}$ pure sliding speed and a 25 bar vertical load. The addition of pressure on a sliding locked block may increase temperature, however, increasing the pressure (load) on a free-rolling tire during touchdown will actually reduce the temperature by reducing the slip distance.

In [16], an aircraft tire in cornering modeled using finite element software and experimental devices for pure sliding rubber. They tested the fully skidding wheel under a 250 kN constant vertical load and a $50\ \text{km/h}$ sliding speed to estimate heat generated by friction. However, the tire tread temperature increased significantly to $190\ C^o$ when the tire slid over a 4 m distance. This result is useful to check heat generated by our model.

In early research, NASA did some simulations to estimate tire tread temperature during the skidding phase. They found that the average was 800 F ($426\ C^o$) [17]. Another test by NASA found that the tread temperature reached $315\ C^o$ [18]. However, the advantage of our model presented is that it simulates the real landing with touchdown speeds,

including sink rate. It also has the wheel connected with a shock absorber to find the damping force and the wheel's dynamic behavior.

II. Modeling and Simulation

The following assumptions were made in order to simplify the model and because the evaluation includes constructing the same underlying assumptions for all wheel statuses. First, after touchdown, the pilot does not use brakes in order to prevent the wheels from skidding [19]. Further, constant horizontal speed was used, and the aircraft will land with all of the main wheels and zero wing lift [20, 21]. Moreover, the maximum aircraft landing weight was used. Also, roughly two seconds after the main wheels land, the nose wheel will touch the ground [22]. Therefore, the aircraft weight is divided by the number of rear wheels only.

A. Aircraft Speed

The typical aircraft approach technique is to preserve a constant speed in order to reach 50 feet (15 m) over the edge of the runway prior to the flare maneuver. The flare is used to decrease vertical speed, complete a smooth landing, and to lessen the landing distance. While the flare maneuver is being conducted, the vertical speed is inconstant, and the pitch angle is increased in order to bring enough drag and slow the aircraft by about 10 knots [23]. The vertical sink rate at the moment of landing for the Boeing 747-400 aircraft usually fluctuates between 1.5 m/s and 3 m/s [24]. A sink rate of 2.5 m/s is used at the beginning of each landing simulation in this study except during sensitivity tests. The horizontal speed at landing is equal to the approach speed of the Boeing, 80.78 m/s, minus 5.14 m/s from a decrease in speed caused by the flare. This results in a horizontal touchdown speed of 75.6 m/s [23, 25]. Moreover, two sensitivities are used: horizontal speed sensitivities of 60 m/s and 90 m/s, and sink rate sensitivities of 1 m/s and 5 m/s.

B. Landing Gear Dynamics

The simple mass-spring-damper is modelled using the ANSYS mechanical transient as shown in Fig. 1. F_y is equal to the weight applied on the shock absorber because zero lift is assumed at touchdown [26, 27]. Balancing forces vertically, the equation representing oscillation of the vehicle mass in Fig. 1 is:

$$F_y = m\ddot{y} + c\dot{y} + ky \tag{1}$$

The lumped mass vertical displacement, y has an initial value equal to zero at the moment of touchdown. For this model, further assumptions are taken into consideration: the tire is always in contact with the runway surface, the system is under

damped, initial vertical velocity of the wheel axle mass is zero, ($\delta(0) = 0$), and in the initial state, both springs are un-deformed, $y(0) = 0$, $\delta(0) = 0$.

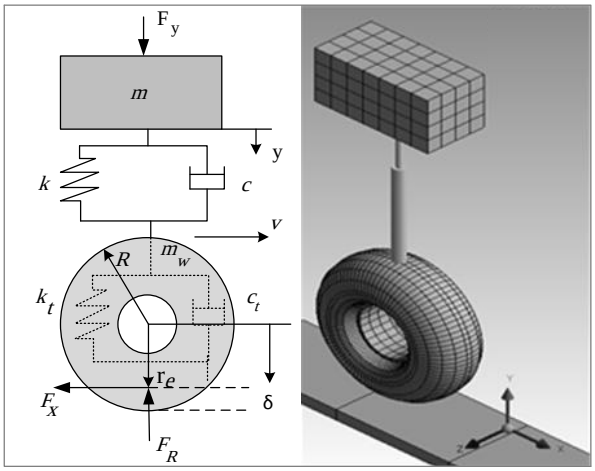

Fig. 1 Mass-spring-damper system (left) and ANSYS model (right).

The equation of motion should be written as [28]:

$$\begin{bmatrix} m & 0 \\ 0 & m_w \end{bmatrix} \begin{Bmatrix} \ddot{y} \\ \ddot{\delta} \end{Bmatrix} + \begin{bmatrix} c & -c \\ -c & (c_t + c) \end{bmatrix} \begin{Bmatrix} \dot{y} \\ \dot{\delta} \end{Bmatrix} + \begin{bmatrix} k & -k \\ -k & (k_t + k) \end{bmatrix} \begin{Bmatrix} y \\ \delta \end{Bmatrix} = \begin{Bmatrix} F_y \\ 0 \end{Bmatrix} \quad (2)$$

In our case study, the wheel mass, m_w is very small compared with total mass, m, so it is ignored.

The reaction force acts vertically on the tire contact patch, F_R is equal to the weight applied on the wheel; and to the tire damping coefficient, c_t multiplied by the tire deflection rate, $\dot{\delta}$ plus the tire linear stiffness, k_t multiplied by the amount of tire deflection δ, to be written as:

$$F_R = c_t\dot{\delta} + k_t\delta \quad (3)$$

In a static condition, the tire deflection rate $\dot{\delta}$ is equal to zero. So, $F_R = k_t\delta$. From this relationship, we can chose the proper stiffness for the tire material and the proper inflation pressure to control the vertical tire deflection ($k_t = 1{,}751{,}268$ N/m and $c_t = 22$ Ns/m) [29]. Solving Eq. (2) for y and δ, using the initial conditions mentioned in the assumptions would give a solution that could be used for determining its first derivative. Including expressions for the final solution for $\dot{\delta}(t)$ and $\delta(t)$ in Eq. (3) would give an expression for change of reaction force in time $F_R(t)$. In this equation, aircraft weight should be included, which applies static force on the system. After sufficient time, when damping overtakes all harmonic oscillations, the final reaction force over the tire contact patches will be equal to the downward force reacting on the landing gear structure: $F_R = F_y, \ (t \to \infty)$

For contact friction, a simple coulomb friction model is used to calculate the friction force, F_x to be:

$$F_x = \mu F_R \tag{4}$$

The friction coefficient, μ is a function of the aircraft's horizontal ground speed, v, and wheel slip, λ:

$$\mu(v, \lambda) = \frac{F_x}{F_R} \tag{5}$$

C. Wheel Translational and Rotational Dynamic

The effective radius of the wheel under the immediate loading conditions should be used, which can be calculated using the radial tires deflection formula [30]. The effective tire radius, r_e is equal to the free wheel radius, R minus a third of the tire deflection, δ to be:

$$r_e = R - \frac{\delta}{3} \tag{6}$$

The friction force, F_x is distanced from the wheel's axle by the effective radius. Utilizing the rotational form of Newton's 2nd law with respect to the wheel moment of inertia I, rotational acceleration of the wheel will be:

$$\dot{\omega} = \frac{F_x r_e}{I} \tag{7}$$

Wheel speed, ω with time is simply calculated as the integral of Eq. (7) with respect to time, plus an initial wheel velocity, ω_i :

$$\omega = \int \dot{\omega}\, dt + \omega_i \tag{8}$$

Figure 2 describes four stages of wheel behaviour at touchdown within a fraction of a second, which is a combination of translational and rotational motion. At position A, the wheel just landed and it is at full skid, $\omega = 0$, and then it will slide for distance Δx to position B. We can calculate the distance, Δx at any position by knowing the sliding time because v is constant ($\Delta x = \Delta t\, v$). From position A to B, the tire contact patch will not change, so the circumference of the tire's sliding distance at contact with the runway, Δc is just the tire contact patch. Thus, $\Delta x \gg \Delta c$, and the relative velocity between a point tangential to the outer tire surface "skidding speed, v_s" is equal to the forward speed of the aircraft, v:

$$v_s = v \tag{9}$$

The second stage is when the wheel starts to spin-up from position B as it is effected by a high friction force, F_x, to reach the free rolling level at position C. In this stage, $\omega > 0$, $r_e\omega \leq v$, $\Delta x > \Delta c$, and the skidding speed is:

$$v_s = v - r_e\omega \tag{10}$$

The third stage is between the positions C and D, which is referred to as slipping. At this stage, the wheel is already rolling and towed by the aircraft structure to match its forward speed; at the same time, the shock absorber and the tire are fully compressed, which means less wheel effective radius (torque arm). Also, the friction force between the tire and runway has reached its peak value, therefore, the wheel's angular velocity has increased suddenly to be higher than the free rolling level, $r_e\omega > v$ and therefore, the tire's circumference distance is higher than the forward distance of aircraft $\Delta x < \Delta c$. In this case, the skidding speed will be:

$$v_s = r_e\omega - v \tag{11}$$

At the fourth stage, the wheel is settled down to the free rolling level after position D to the end of the runway.

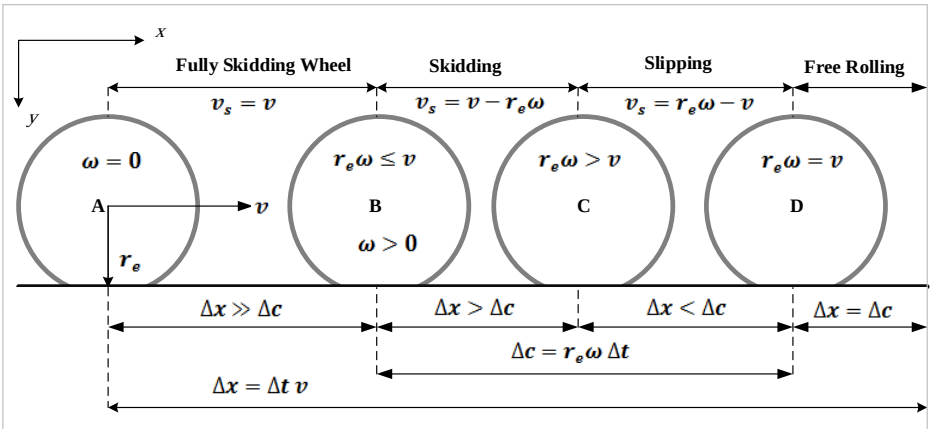

Fig. 2 Four stages of wheel behaviour at touchdown within a fraction of second.

However, based on previous wheel behaviour, the longitudinal wheel slip ratio, λ, is defined as:

$$\lambda = \frac{v_s}{v} \tag{12}$$

Substituting Eq. (9), Eq. (10), and Eq. (11) in Eq. (12) to present different wheel slippage behaviour [31]:

$$\lambda = \begin{Bmatrix} \frac{v}{v} = 1 & \text{if} \quad \omega = 0 \quad \text{(fully skidding wheel)} \\ \frac{v - r_e\omega}{v} & \text{if} \quad r_e\omega \le v \quad \text{(skidding)} \\ \frac{r_e\omega - v}{v} & \text{if} \quad r_e\omega > v \quad \text{(slipping)} \end{Bmatrix} \tag{13}$$

At a high slip ratio, the tire's temperature at its contact surface becomes higher and the friction coefficient becomes lower. However, the landing speed has a larger effect on the friction coefficient than the temperature [32].

Using Burckhardt friction model to estimate the tire runway friction coefficient as a function of longitudinal wheel slip and horizontal ground speed to be [33]:

$$\mu(v, \lambda) = [C_1\left(1 - e^{-C_2\lambda}\right) - C_3\lambda]e^{-C_4\lambda\, v} \tag{14}$$

C_1 is the friction curve maximum value, C_2 is the friction curve shape, C_3 is the difference between the maximum value at $\lambda = 1$ and the maximum value of the friction curve, and C_4 is in the range of $0.02 - 0.04$ s/m.

In this paper, we are using the dry concrete parameters which are: $C_1 = 1.2801$, $C_2 = 23.99, C_3 = 0.52$, and we assume $C_4 = 0.03$ s/m. Figure 3 shows $\mu - \lambda$ curves with different horizontal touchdown speeds. In this model, constant friction coefficient of 0.7, 0.65, and 0.6 were used for the speeds of 60 m/s, 75.6 m/s, and 90 m/s respectively. These are based on the range of values at $\lambda = 0.05 - 0.15$, which many manufactures are using.

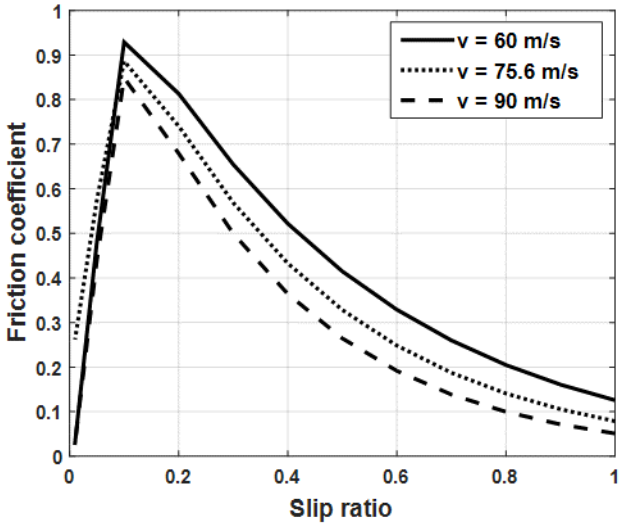

Fig. 3 Relationship between μ and λ at different horizontal landing speeds.

D. Tire Heat Generation

There are two ways that heat is generated by tires: a friction phenomenon caused by sliding the tire under a heavy load and the stress deformation cycle. In this paper, we focus on sliding friction, which is very high compared with other sources. At landing impact, the tire is sliding similar to a block of rubber under a vertical force on the same contact area. This leads to very high heat produced by friction power, in this case, the heat source, q is defined as:

$$q = \frac{F_x v_s}{A_c} \tag{15}$$

A_c is the tire contact area (m^2), which is constant at for a fully skidding wheel and then become changeable [34]. Boeing provides a formula to calculate the tire contact area. This is done by dividing the load per tire by the tire inflation pressure. The tire footprint area is a 1.6 ellipse to be calculated as: minor axis $= 0.894\sqrt{A_c}$, and then the major axis $=$ 1.6 x minor axis [35].

Once the tire starts to spin-up, the contact area will be changed to a new contact area that is not heated yet, and the slip ratio becomes less, which means less heating for the new tire area. Moreover, the initial contact area, which already has been heated to the maximum temperature level, will decrease in temperature as it comes in contact with the new "cold" runway area and cool air. This means that the maximum tire tread temperature will only occur on the initial contact surface while the wheel is fully skidding [15]. Moreover, Eq. (15) is the total heat source and part of this thermal power will transfer to the tire and part will transfer to the runway. Therefore, a partition coefficient, P_c should be used to multiply by the heat source equation. The partition coefficient is governed by the thermal conductivities and diffusivities of the tire, k_t , α_t and runway, k_r , α_r respectively and it can be written as [34]:

$$P_c = \frac{k_t}{k_r}\sqrt{\frac{\alpha_r}{\alpha_t}} \tag{16}$$

Thermal diffusivity, α can be expressed with respect to the material density, ρ; thermal conductivity, k; and the specific heat, c_v to be as:

$$\alpha = \frac{k}{\rho\, c_v} \tag{17}$$

Because all heat source parameters are functions of time, by adding the partition coefficient in Eq. (16) to Eq. (15), the tire heat source becomes as follows:

$$q_t = P_c \int \frac{1}{A_c}\, dt \int F_x\, dt \int v_s\, dt \tag{18}$$

E. Simulation Setup

The model consists of five parts: the tire, the rim, the shock absorber, the weight box, and the runway as shown in Fig. 4. Using ANSYS design modeler, the tire has been modeled as one material because the goal of this project is to estimate temperature on the first layer of the tire tread only. The 5180 nodes and 2286 elements are used to mesh the tire and it was filled to 215 PSI. The rim has been added to the tire to control its weight by increasing or decreasing its density to obtain the correct wheel mass. A shock absorber has been connected from the center of the rime to the weight box. Its position is vertical to avoid any cornering, it has the same properties as a Boeing 747-400 shock absorber and is valid for a single wheel ($k = 3.12x10^5$N/m and $c = 3.42x10^5$ Ns/m) [20].

The weight being applied on the wheel is 18484 kg, which is found by taking the maximum landing weight of a Boeing 747-400, which is 295,743 kg divided by 16 (number of rear wheels) [25]. Finally, the runway is designed to be long enough to complete the simulation.

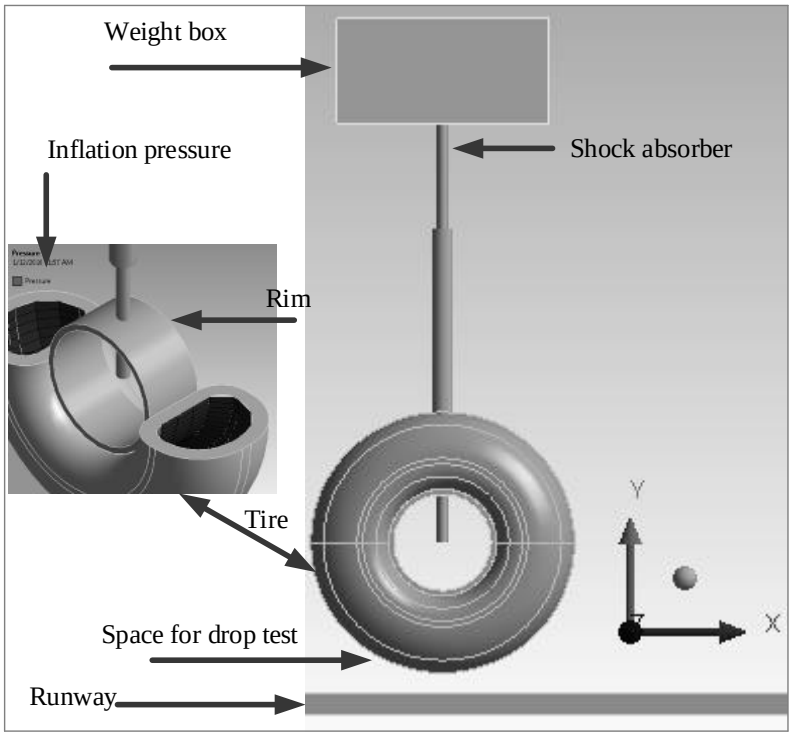

Fig. 4 Geometry of parts: tire, shock absorber, weight box, rim, and runway.

ANSYS mechanical transient can simulate the dynamic behavior, but to find the heat generated by friction, we have to use a coupled field structural-thermal analysis. In this case, we are supposed to use elements that support combined structural-thermal. ANSYS provides several solid elements that have these properties. "Solid226" is used for this model by applying the command (APDL) for the tire and runway contact surfaces. The users defined results of "TEMP" and "OMGZ" were chosen for tread temperature and wheel angular velocity respectively. At frictional contact between the tire and runway, the simulation provides the forces for every time step. During transient analysis in each time step, there is a small increment of wheel sliding or angular displacements applied, so it is important to apply a small time step ($dt = 1x10^{-6}sec$). Table 1 shows the 3D Main landing gear wheel geometry data [36, 37]. The tire rubber is hyper elastic material, which is defined based on the standard material model available in ANSYS. Table 2 shows the tire tread material properties [16]. Mooney- Rivlin material model has been considered because the tire tread contains a rubber compound with available constants. The material constants defined for Mooney – Rivlin model is supported with the

stress versus strain curve for the material, which helps to capture the failure behavior of the tire. The runway is modeled as being of concrete material with a flat surface, and no texture. The partition coefficient, P_c is assumed to be 0.9, which means 90% of heat flux goes to the tire and only 10% goes to the runway.

Table 1 Wheel geometry data

	Weight (kg)	**Diameter (mm)**	**Width (mm)**
Tire	110	1244.6	482.6
Rim	74.4	510	457.2

Table 2 Material parameters of tire tread

Properties	**Value**
Passion's ratio	0.49
Mass density ($\mathbf{kg/m^3}$)	1125
Mooney Rivlin constants (Mpa)	$C_{10} = 0.643$, $C_{01} = 0.824$
Thermal conductivity ($\mathbf{W/mC^o}$)	1900
Specific heat ($\mathbf{J/kgC^o}$)	0.2

III. Results and Discussion

A. An Initial Verification

For an initial check of the temperature results, we simulated the tire sliding on the runway without its shock absorber or box weight, and we applied 250 kN vertically on the rim using a constant friction coefficient of 0.65. The speed was set at 13.89 m/s ($50\mathrm{km/hr}$) in order to capture the temperature after 4m of sliding distance. Figure 5 shows the tire force and a temperature profile of 186.4 C^o, which is in very good agreement with an error of only 2.36% compared with a temperature value of 190.9 C^o, which was achieved in [16].

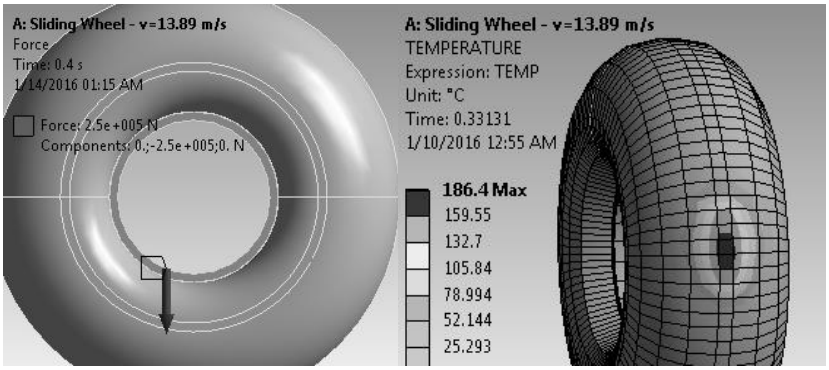

Fig. 5 Pure sliding tire force and temperature profile.

B. Wheel Dynamic Behavior

From first simulation for the static wheel with $\omega_i = 0$, we obtained the wheel free- rolling angular velocity when it reached to a steady state to set the 50% and 100% pre-rotation wheel for the 2nd and 3rd simulations respectively. Figure 6 shows the tire deflection at landing impact. We can simply calculate the amount of tire deflection at a steady state using Eq. (6); however, the wheel angular velocity is enough to set the pre-rotation.

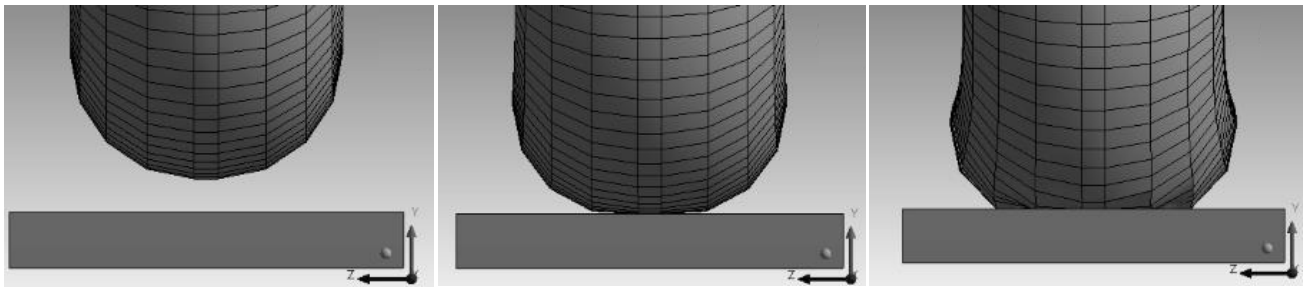

(a) **(b)** **(c)**

Fig. 6 Tire landing impact: (a) Approach, (b) Touchdown, and (c) Deflection.

For the three simulations, the reaction force, F_R is similar because the same weight and vertical speed are used, and also the pre-rotation wheel does not make significant changes. Figure 7 shows the vertical and longitudinal forces reacted at a single wheel contact patch versus time during landing, as shown, the peak value of the reaction force is occurred within 0.055 seconds. At this time, the shock absorber is completely compressed, and the tire is at the maximum deflection rate, δ. The reaction force is decreased later because it was effected by the shock absorber and tire damping.

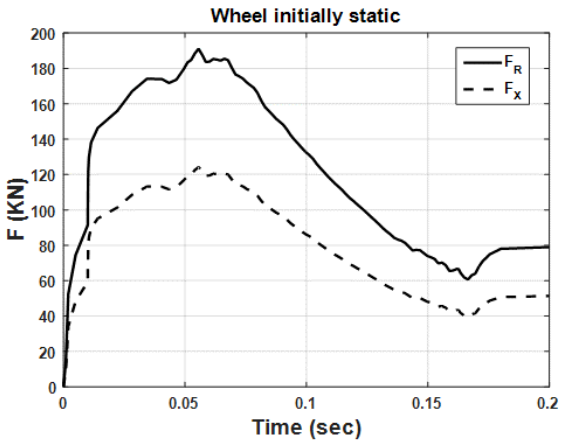

Fig. 7 Reaction and friction forces vs. time

(Initial horizontal speed = 75.6 m/s, initial sink rate = 2.5m/s).

The longitudinal force, F_x follows the reaction force behaviour because a constant friction coefficient is used to avoid model complexity. The friction force increased immediately after touchdown and reached its peak value when the shock absorber and the tire were fully compressed. During the increase in the friction force, the wheel was still at full skid within fractions of a second as it was pulled out by the high forward aircraft speed to cover the full slip distance, until the friction force spun it. At the peak value of the friction force, the wheel spun-up to overshoot level as it was already rolling and affected by the sudden extra friction force. Figure 8 presents the minimum and the maximum wheel angular velocities for the three simulations (the negative sign represents – z axis).

Figure 9 shows a comparison of wheel angular velocities and slip ratios with initial rotational speeds. The initially static wheel was at full skid for 0.033 sec with a distance of 2.49 m. Then the wheel started to spin-up and the total skidding distance was 9.1 m during 0.12 sec. This agreed with the results in [12] and [13]. The curve shows the wheel spin-up is more than the free-rolling level at 140.4 rad/sec. This is because it was towed to rotate and match the aircraft forward speed; and the friction force reached the peak value which spun the wheel to overshoot level, and then the wheel wavered to spin-down to reach a velocity where $\omega r_e = v$, i.e. the slip ratio can be zero when the aircraft forward speed is equal to the tangential velocity of a point on tire's surface. When this occurs, the wheel spin-up phase has ended, and the tire is able to rolling without interference until breaks are used to slow the wheel. In the first simulation, the wheel free rolling velocity at a steady state was 121 rad/sec. Therefore, this value was set for the 100% pre-rotation, and 60.5 rad/sec was used for the 50% pre-rotation value.

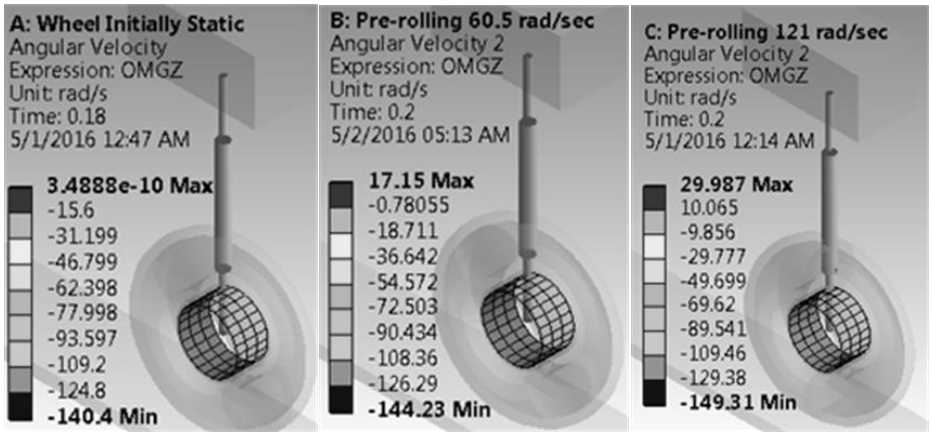

(a) **(b)** **(c)**

Fig. 8 Minimum and maximum angular velocities for; (a) wheel initially static, (b) 50% pre-rotated wheel, and (c) 100% pre-rotated wheel.

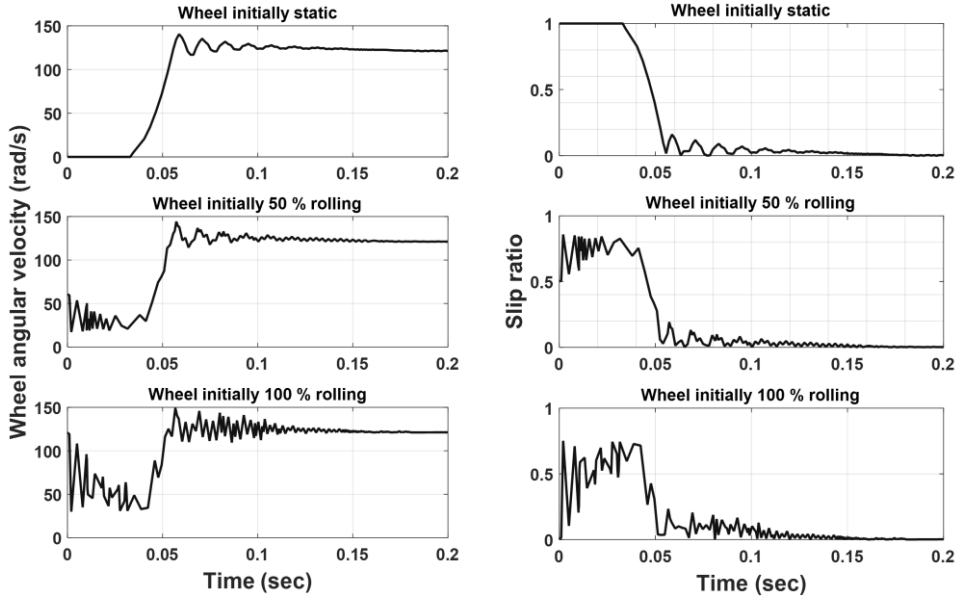

(a) **(b)**

Fig. 9 (a) Angular velocities vs. time for; initially static, 50% and 100% pre-rotated wheel, (b) Slip ratios vs. time for; initially static, 50% and 100% pre-rotated wheel (initial horizontal speed, $v = 75.6\ m/s$, initial sink rate $= 2.5\ m/s$).

The wheel initially rolling at 50% shows a drop in velocity at the moment of contact with the ground from 60.5 to 17.15 rad/sec within 0.002 seconds. It only waivered for 0.05 seconds with an average of 30 rad/sec. The friction force

became high enough to spin it to overshoot more than wheel's initial static level to 144.23 rad/sec, which is logical as it rotates and is effected by the same effects that occur for a typical landing wheel. However, the steady state rotation was achieved after 0.13 seconds with slight slipping until 0.14 seconds, and the total distance was 9.83 m.

The wheel initially rolling at 100% pre-rotation also shows a drop at landing impact from 121 to 30 rad/sec within 0.002 seconds. The wheel wavers for 0.04 seconds to spin up to its highest level at 149.31 rad/sec. It settled down to be free rolling after 0.14 seconds with a 10.58 m skidding distance.

Figure 9 (b) shows that when the wheel was initially static it slipped 100% during full skid of the wheel, and it became zero at a steady state. The maximum value of a 50% pre-rotating wheel was 0.86 of slippage. It increased from 0.5 to 0.72 immediately after touchdown within 0.002 seconds, and it maintained an average value of 0.75 for 0.04 seconds. The 100% pre-rotating wheel slip increased within 0.002 seconds from zero to 0.75, and then it wavered with an average value of 0.5 for 0.05 seconds. The comparison shows the lowest average slip was for 100% pre-rotated wheel, but the angular velocity range was the highest. A fully skidding wheel is avoided by pre-rotating the wheel by 50%, but the slip still occurred even with a fully rotational speed. This simulation did not provide torque applied to the spinning wheel before touchdown, and for this reason, it is possible that the reduction of the pre-spun wheel's angular velocity is high.

C. Tire Tread Temperature

The maximum values of tread temperatures for the three simulations are shown in Fig. 10. The initially static wheel, in Fig. 10 (a), recorded the highest temperature on its first contact area with the runway at $307.41\ C^{o}$. The small area surrounding the wheel had a temperature of $260\ C^{o}$, and the majority of tread temperature was less than $165\ C^{o}$. The static wheel had the highest temperatures because the affected area was fully sliding with a speed equal to the aircraft's forward speed until the longitudinal friction force increased to spin the wheel and then changed its position. The hottest spot represents the most affected area, and it became sticky and wear occurred easily. Also, the temperature of the surrounding area exceeded the rubber melt temperature. The spin up time was not enough to increase the tire's circumference area to a high temperature even though the slip was high during spin up. The temperature decreased by convection due to periods of noncontact for each wheel revolution. Moreover, the tread contacted new cold runway areas that decreased the temperature as well. The fall in temperature appears after the spin-up phase has ended, because it is small compared to the increase in temperature due to the high slip.

In Fig. 10 (b), the tire tread temperature of the wheel initially rolling at 50% shows a reduction in maximum value. The high temperature was on the area of first contact with the runway, which increases with every wheel rotation to be the highest when compared with the tire's circumference. The spin up time was enough to increase the tread temperature to 193.49 C^o, and because the tire was not at full skid, the affected area was larger with less temperature compared with the initially static wheel.

In Fig. 10 (c), the tire that was initially fully rolling does not show a high reduction of its tread temperature. This is because its slip ratio reached a high level of 75% after touchdown. Also, its maximum temperature was 159.69 C^o on its first contact area. Figure 11 shows tire tread temperature comparisons, in all simulations, there was a delay in heat flux because the dynamic movement was very fast, and this was followed by an increase in temperatures.

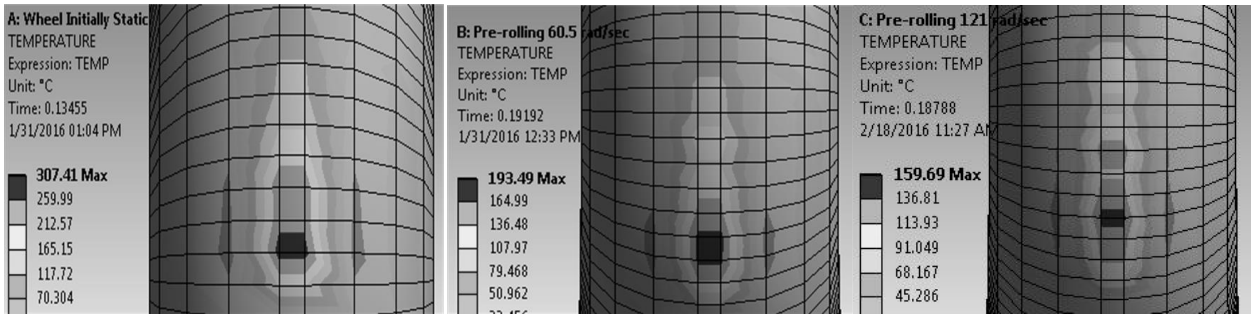

(a) **(b)** **(c)**

Fig. 10 Maximum value of tread temperature for (a) wheel initially static, (b) 50% pre-rotated wheel, and (c) 100% pre-rotated wheel.

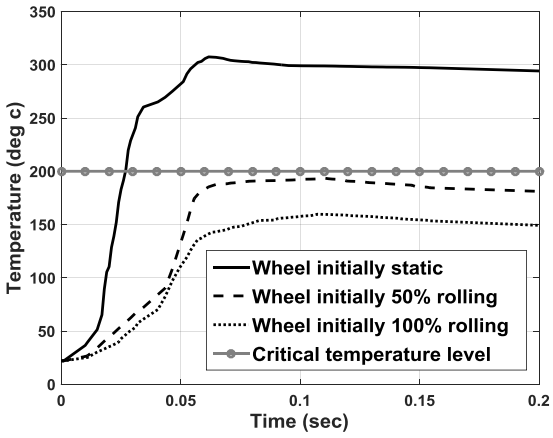

Fig. 11 Tire tread temperature vs. time for wheel initially static, 50% pre-rotated wheel, and 100% pre-rotated wheel.

D. Horizontal Speed Sensitivity

With the same inputs, tests were conducted for an initially static wheel with different landing speeds, $v = 60$ m/s and 90 m/s. Figures 12-14 shows reaction and friction forces, wheel angular velocities, and temperature level curves respectively. The friction force at the low speed of 60 m/s is higher and increased immediately. This reduced the fully skidding wheel distance (comparing with $v = 75.6$ m/s) to 1.2 m (48% less). Also, the wheel spun up to the maximum value 114.08 rad/sec within 0.052 seconds, and the total skidding phase distance was reduced by 14% to be 7.8 m within 0.13 seconds.

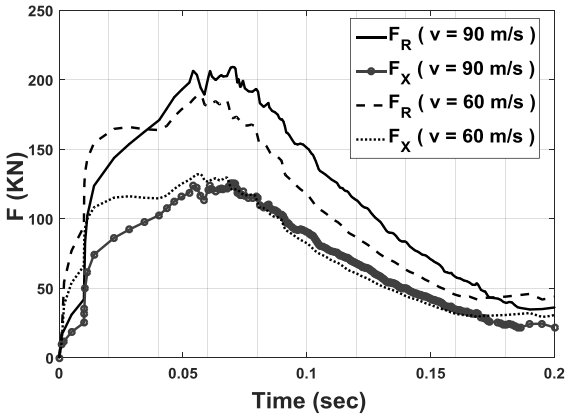

Fig. 12 Reaction and friction forces vs. time for different landing speeds $(\mathbf{sink\ rate = 2.5 m/s})$**.**

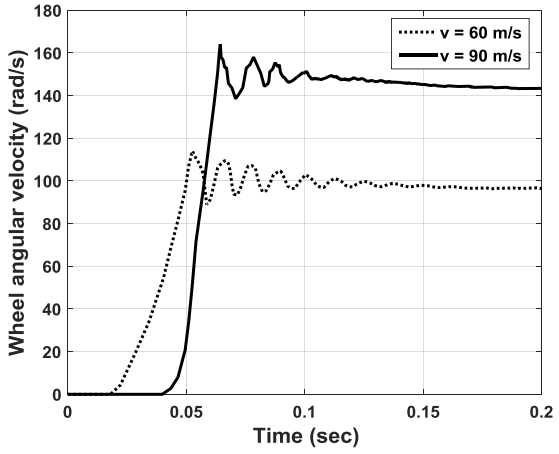

Fig. 13 Wheel angular velocity vs. time for different landing speeds $(\mathbf{sink\ rate = 2.5 m/s})$.

At the high speed of 90 m/s, the wheel slid longer and was effected by low friction and a high gap between translational and zero rotational speed. The wheel slid for 3.59 m (31% higher), and the total skidding distance increased by 16% to be 10.8 m. The wheel angular velocity reached its peak value at 164.02 rad/sec within 0.064 seconds and settled down after 0.12 seconds. Figure 15 shows the maximum wheel angular velocities and tread temperature values. The temperature at the low speed was reduced to 241.3 C^o(21.5% less) while at the high speed it reached 359.31 C^o (14.4% higher).

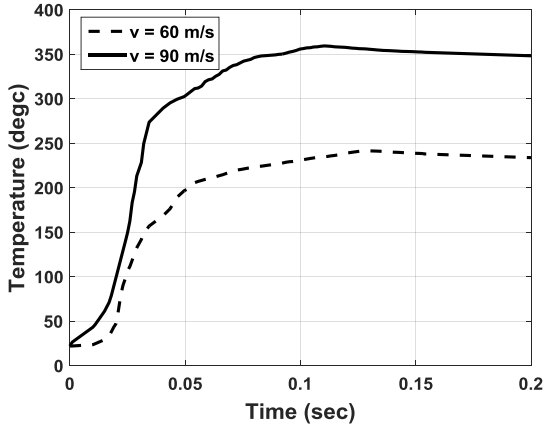

Fig. 14 Tire tread temperature levels vs. time for different landing speeds (sink rate $= 2.5\mathrm{m}/\mathrm{s}$).

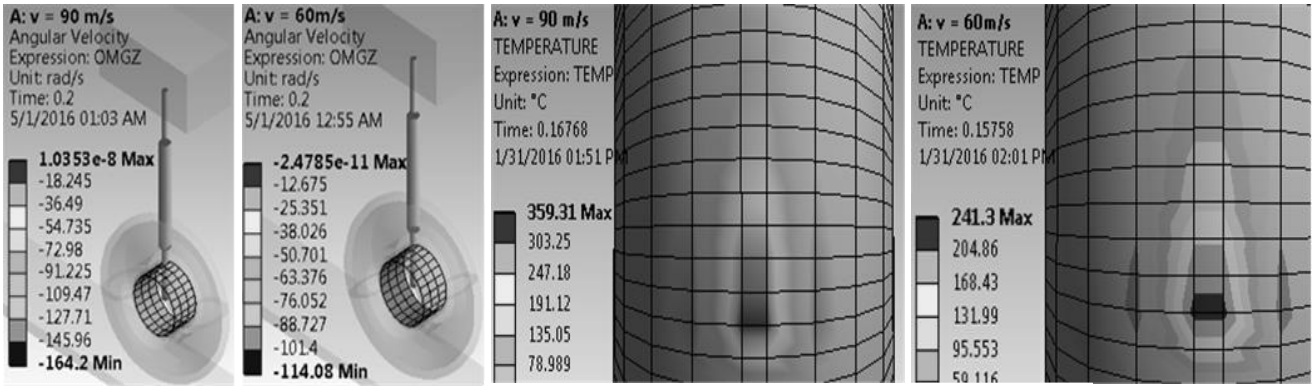

(a) (b) (c) (d)

Fig. 15 Maximum and minimum wheel angular velocity values for initial landing speeds; (a) $v = 90\ m/s$, (b) $v = 60\ m/s$ and maximum temperature levels for initial landing speeds; (c) $v = 90\ m/s$, (d) $v = 60\ m/s$ (initial sink rate of 2.5 m/s).

E. Vertical Speed Sensitivity

Vertical speed (sink rates) sensitivity was tested also using 5 m/s for a hard landing and 1 m/s for a smooth landing with a 75.6 m/s horizontal speed. Figures 16-18 shows reaction and friction forces, wheel angular velocities, and temperature curves respectively. The hard landing shows a lower temperature because high friction occurred immediately, which reduced the fully skidding wheel time to 0.014 seconds and the distance to only 1.06 m (42% less than typical landing). The total skidding time and distance increased to be 0.13 seconds and 9.83 m respectively. This was because the wheel spun up to 153.67 rad/sec, which is 9% higher than a typical landing. Furthermore, the tread temperature reduced to 284.38 C^o (7% less) as the time when the wheel is at full skid is reduced.

The soft landing data shows a delay in longitudinal friction that led to skidding a longer distance. The wheel started to spin up after 0.039 sec with a distance of 2.95 m, but the temperature reached to 288.65 C^o, which is less than a typical landing (6%). This is because the friction force is less than the typical landing. This appeared with the peak value of wheel angular velocity, which reached 134.76 rad/sec with a relatively long spin up time. The total skidding time and distance was 0.14 seconds and 10.58 m respectively.

Figure 19 shows the tire tread temperature and angular velocities profiles. The hard landing led to high tire deflection, which resulted in a large hot spot area compared with a typical and soft landing.

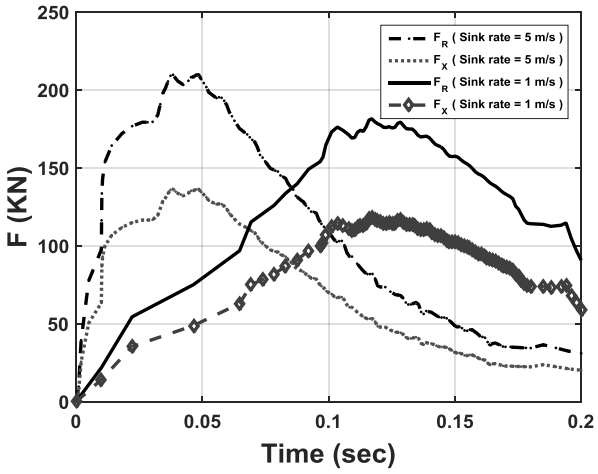

Fig. 16 Reaction and friction forces vs. time vs. time for different sink rates (initial horizontal speed, $v = 75.6\ m$).

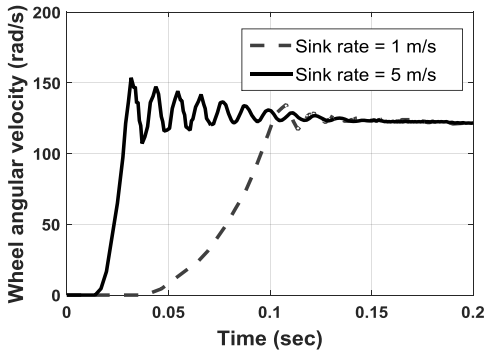

Fig. 17 Wheel angular velocity vs. time for different sink rates.

(initial horizontal speed, $v = 75.6\ m$).

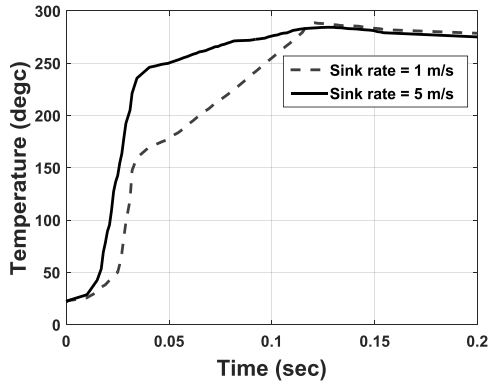

Fig. 18 Tire tread temperature vs. time for different sink rates

(initial horizontal speed, $v = 75.6\ m/s$).

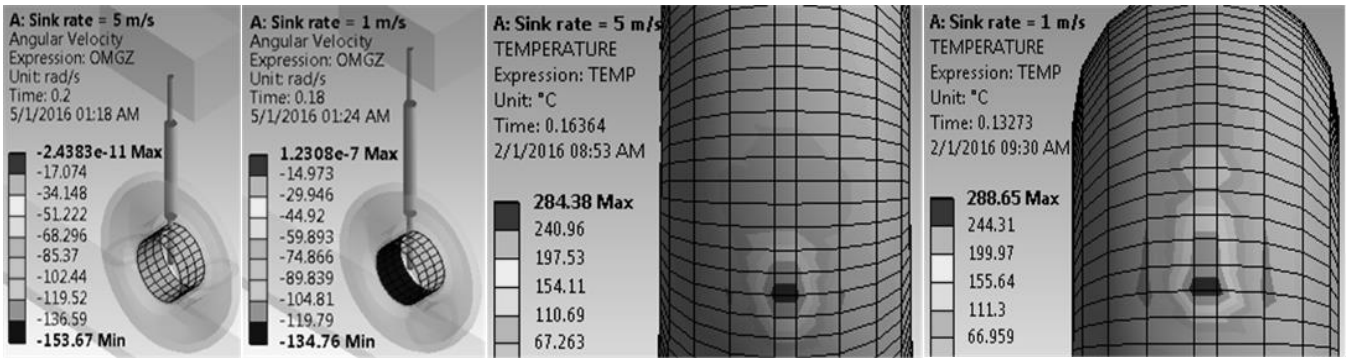

(a) (b) (c) (d)

Fig. 19 Maximum and minimum wheel angular velocity values for different initial sink rates; (a) 5 m/s, (b) 1 m/s and maximum temperature levels for different initial sink rates; (c) 5 m/s, (d) 1 m/s

(initial horizontal speed of 75.6 m/s)

F. Summary of Results

For all simulations, Table 3 presents the skidding time and distance, maximum slip ratio, and the maximum tread temperatures with input data:

Table 3. Summary of results

ω_i (rad/sec)	v (m/s)	Sink rate (m/s)	Max. ω (rad/sec)	Min. ω (rad/sec)	Fully skidding wheel distance (m)	Fully skidding wheel time (sec)	Spin-up/ down distance (m)	Spin-up/down time (sec)	Total skidding distance (m)	Total skidding Time (sec)	Max. Slip ratio	Max. Temp. C^o
0	75.6	2.5	140.4	0	2.49	0.033	6.58	0.087	9.1	0.12	1	307.41
60.5	75.6	2.5	144.23	17.15	0.0	0.0	9.83	0.13	9.83	0.13	0.86	193.49
121	75.6	2.5	149.3	29.99	0.0	0.0	10.58	0.14	10.58	0.14	0.75	159.69
0.0	90	2.5	164.02	0.0	3.59	0.039	7.2	0.08	10.8	0.12	1	359.31
0.0	60	2.5	114.08	0.0	1.2	0.02	6.6	0.11	7.8	0.13	1	241.3
0.0	75.6	1	134.76	0.0	2.95	0.039	7.56	0.10	10.58	0.14	1	288.65
0.0	75.6	5	153.67	0.0	1.06	0.014	8.77	0.116	9.83	0.13	1	284.38

IV. Conclusion

A single wheel of an aircraft's main landing gear has been modeled using ANSYS transient coupled structural-thermal to calculate the reduction of tire tread temperature that can be achieved by pre-rolling the wheel before touchdown. The model shows results of the tire tread temperature immediately after touchdown for a typical landing (where the wheel is initially static), 50% and 100% pre-rotated wheel, the sensitivity to the horizontal landing speeds and the sensitivity to sink rates.

We conclude that rotating the aircraft wheel before landing to 50% of its free rolling velocity on the runway could reduce the tire tread temperature at touchdown to be below the rubber's critical temperature.

The angular velocity of the pre-rotated wheel decreases immediately after touchdown, but full skid is avoided and the tire produces heat as the slip occurs, even with a fully pre-rotated wheel.

Increasing the horizontal landing speed increases the tire tread temperature and vice versa. A hard landing increases the load on the wheel at touchdown, which leads the wheel to spin-up faster, due to a higher level of friction between the

tire and runway compared with the level for a typical landing; thus, the less the skidding distance and time, the lower the tire tread temperature.

In the end, only longitudinal dynamic is modeled in this paper. Further study should include lateral dynamic in the case of cross wind landing.

Appendix A

Theoretical FEM Model

Considering, q_t the source term of the diffusion equation, and its function of time, the diffusion equation in the cylindrical polar coordinate is given by:

$$\frac{\partial T}{\partial t} - \frac{\alpha}{r}\frac{\partial}{\partial r}\left(r\frac{\partial T}{\partial r}\right) - \alpha\frac{\partial^2 T}{\partial y^2} - \frac{\alpha}{r^2}\frac{\partial^2 T}{\partial \theta^2} = q_t(t) \tag{19}$$

Figure 20 shows the cylindrical polar coordinate system for the tire tread contact with the runway, which is unchangeable at full skid wheel and changeable during spin-up or rotation. In spin-up case, the cold tread material is coming in, and the heated tread is going out for some time step.

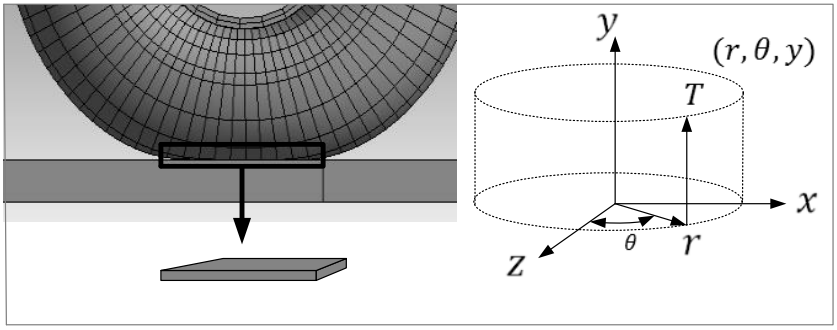

Fig. 20 Cylindrical polar coordinate system for tire tread contact with the runway.

However, for every sub-region we assume element wise angular symmetry around every material point of the contact tread. This assumption helps us to solve the problem on a 2-D domain. The 2-D schematic representation of tread is given by Fig. 21. We let T donate the temperature inside the tread at any given point in the tread at time *t*.

The temperature is modeled to satisfy the diffusion equation on the 2-D schematic representation of the domain as follows: r is the radial variable in the cylindrical polar coordinates, y is the vertical space variable in the cylindrical polar coordinates, q_t is the source term, which donates the generated amount of heat that results from the work done by friction.

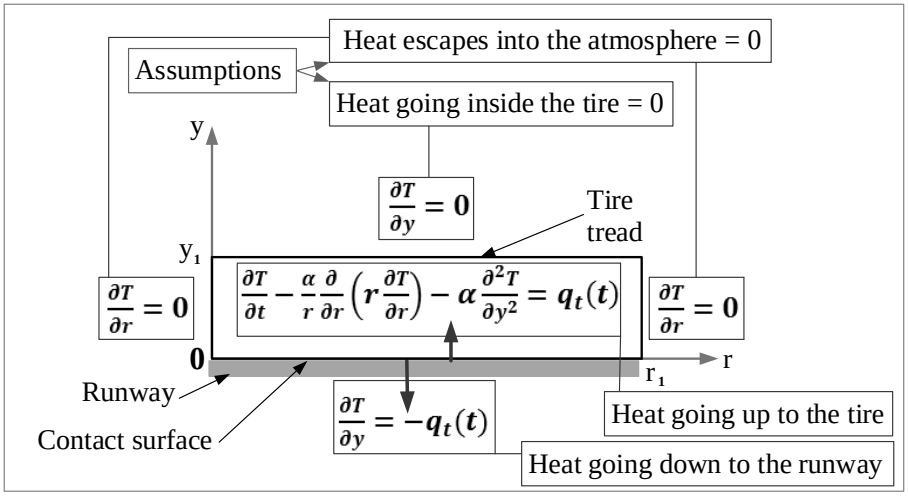

Fig. 21 2-D schematic of tread contact with the runway.

The initial condition for which we assume a certain uniform temperature at the beginning of touchdown is:

$$T(r, y, 0) = T_0(r, y) \qquad 0 < r < r_1, \qquad 0 < y < y_1$$

We use the finite element method to solve this equation. In order to compute the weak formulation, we introduce the solution and test the function spaces by: $H_E(\Omega) = \{v_t : v_t \in H^1(\Omega)$ and v_t satisfies the boundary conditions posed by the problem$\}$, and $H_{E_0}(\Omega) = \{v_t : v_t \in H^1(\Omega), v_t$ is zero on all boundaries$\}$ respectively, where $H^1(\Omega)$ is the set of all functions whose norm and the norm of its first derivative is bounded. We multiply both sides of the equation by a test function $v_t \in H_{E_0}(\Omega)$ and integrate over r and y:

$$\int_\Omega \frac{\partial T}{\partial t} v_t \, dr \, dy - \alpha \int_\Omega \left(\frac{1}{r}\frac{\partial}{\partial r}\left(r\frac{\partial T}{\partial r}\right) + \frac{\partial^2 T}{\partial y^2}\right) v_t \, dr \, dy = \int_\Omega q_t \, v_t \, dr \, dy$$

Using integration by parts we get:

$$\int_\Omega \frac{\partial T}{\partial t} \, v_t \, r \, dr \, dy - \alpha \int_\Omega \left(\frac{\partial T}{\partial r}\frac{\partial v_t}{\partial r} + \frac{\partial T}{\partial y}\frac{\partial v_t}{\partial y}\right) r \, dr \, dy + \alpha \int_{\partial\Omega} v_t \, \frac{\partial T}{\partial n} \, dS = \int_\Omega q_t \, v_t \, r \, dr \, dy$$

where, S is the stiffness and n is the outward normal vector to the boundary. The boundary term will vanish because either v_t is zero on the boundary or $\frac{\partial T}{\partial n}$ is zero, therefore we have:

$$\int_\Omega \frac{\partial T}{\partial t} v_t \, r \, dr \, dy - \alpha \int_\Omega \nabla T . \nabla v_t \; r \, dr \, dy = \int_\Omega q_t \, v_t \, r \, dr \, dy$$

Which can be written as:

$$\int_{\Omega} \left[\frac{\partial T}{\partial t} v_t - \alpha \nabla T . \nabla v_t - q_t v_t\right] r \, dr \, dy = 0$$

The weak formulation of the problem is to find $T \in H_E(\Omega)$ such that:

$$\int_{\Omega} \left[\frac{\partial T}{\partial t} v_t - \alpha \nabla T . \nabla v_t - q_t v_t\right] r \, dr \, dy = 0$$

For all $v_t \in H_{E_0}(\Omega)$. We define the finite element spaces by:

$V_E^h(\Omega) = \{v_h : v_h \in V^h(\Omega)$ and v_h satisfies the boundary conditions posed by the problem $\}$,

$$V_{E_0}^h(\Omega) = \{v_h : v_h \in {V_E}^h(\Omega) \text{ and } v_h \text{ is zero on the boundaries}\}$$

The corresponding finite element formulation is to find $v_h \in V_E^h(\Omega)$ such that

$$\int_{\Omega} \left[\frac{\partial T_h}{\partial t} v_h - \alpha \nabla T_h . \nabla v_h - q_t v_h\right] r \, dr \, dy = 0$$

For all $v_h \in V_{E_0}^h(\Omega)$, we express T_h and v_h in terms of linear combinations of basis functions of the finite element spaces in the form of:

$$T_h = \sum_{i=1}^{N} T_i \emptyset_i \text{ and } v_h = \sum_{j=1}^{N} \emptyset_j$$

Where, T_i is the temperature at the ith node. This will be the vector of unknowns to be computed by the resulted algebraic system. $\emptyset_i$ and $\emptyset_j$ are the basis functions, which from $i, j = 1$ to $i, j = N$ collectively span the finite element space $V_E^h(\Omega)$. Substituting the expressions for T_h and v_h in the finite element formulation we get:

$$\frac{d}{dt}\int_{\Omega} \sum_{i=1}^{N} T_i \emptyset_i \sum_{j=1}^{N} \emptyset_j \, r \, dr \, dy - \alpha \int_{\Omega} \sum_{i=1}^{N} T_i \nabla \emptyset_i \sum_{j=1}^{N} \nabla \emptyset_j \, r \, dr \, dy - \int_{\Omega} q_t \sum_{j=1}^{N} \emptyset_j \, r \, dr \, dy = 0$$

Assuming sufficient smoothness of $\emptyset_i$ and $\emptyset_j$, we may interchange the summation with integration, so we have:

$$\sum_{i,j=1}^{N} T_i' \int_{\Omega} \emptyset_i \emptyset_j r \, dr \, dy - \alpha \sum_{i,j=1}^{N} T_i \int_{\Omega} \nabla \emptyset_i . \nabla \emptyset_j . r \, dr \, dy = \sum_{j=1}^{N} q_t \int_{\Omega} \emptyset_j r \, dr \, dy$$

where, T_i' is $\frac{dT_i}{dt}$. Here the time derivative only hits the coefficient because $\emptyset_i$ is not dependent on time. We may write this as a system of an algebraic equation for each time step. We use the finite difference method to step up in time, and as such, we define the following vectors and matrices:

$S =$ the stiffness matrix and its entries are defined by:

$$[S]_{i,j} = \int_{\Omega} \alpha \nabla \emptyset_i . \nabla \emptyset_j r \, dr \, dy$$

$M =$ the mass matrix and its entries are given by:

$$[M]_{i,j} = \int_{\Omega} \emptyset_i . \emptyset_j r \, dr \, dy$$

$L =$ the load vector and its column entries are given by:

$$[L]_j = \int_{\Omega} q_t \emptyset_j r \, dr \, dy$$

We use backward Euler's scheme to step up in time so we have:

$$T_i' = \frac{T_i^{m+1} - T_i^m}{\Delta t}$$

$$M \frac{T^{m+1} - T^m}{\Delta t} - ST^{m+1} = L^{m+1}$$

$$MT^{m+1} - MT^m - \Delta t S T^{m+1} = \Delta t \, L^{m+1}$$

$$(M - \Delta t S) T^{m+1} = MT^m + \Delta t \, L^{m+1}$$

This is a discrete system of N algebraic equations with N unknown for each time step. When the solution to this system is obtained for every time step, the temperature at every node in the discretized domain of the tread will be known, and one will be able to take into account the consequences of high and low temperatures in different regions within the tread material.

Appendix B

Simulation Process

The main process of the simulation model is shown in Fig. 22. The simulation begins with the input data in the form of variables and invariables. The variable data changes from one simulation to another while the invariable data is constant for all the simulations.

In this model, there are two steps of calculation for each iteration. The first step is the mechanical analysis of the wheel's dynamic behavior and the forces generated at the tire's contact with the runway. In this step, everything needed to calculate the friction power (Eq. 15) is done; i.e. the friction force, the wheel skidding speed and the tire contact area are calculated.

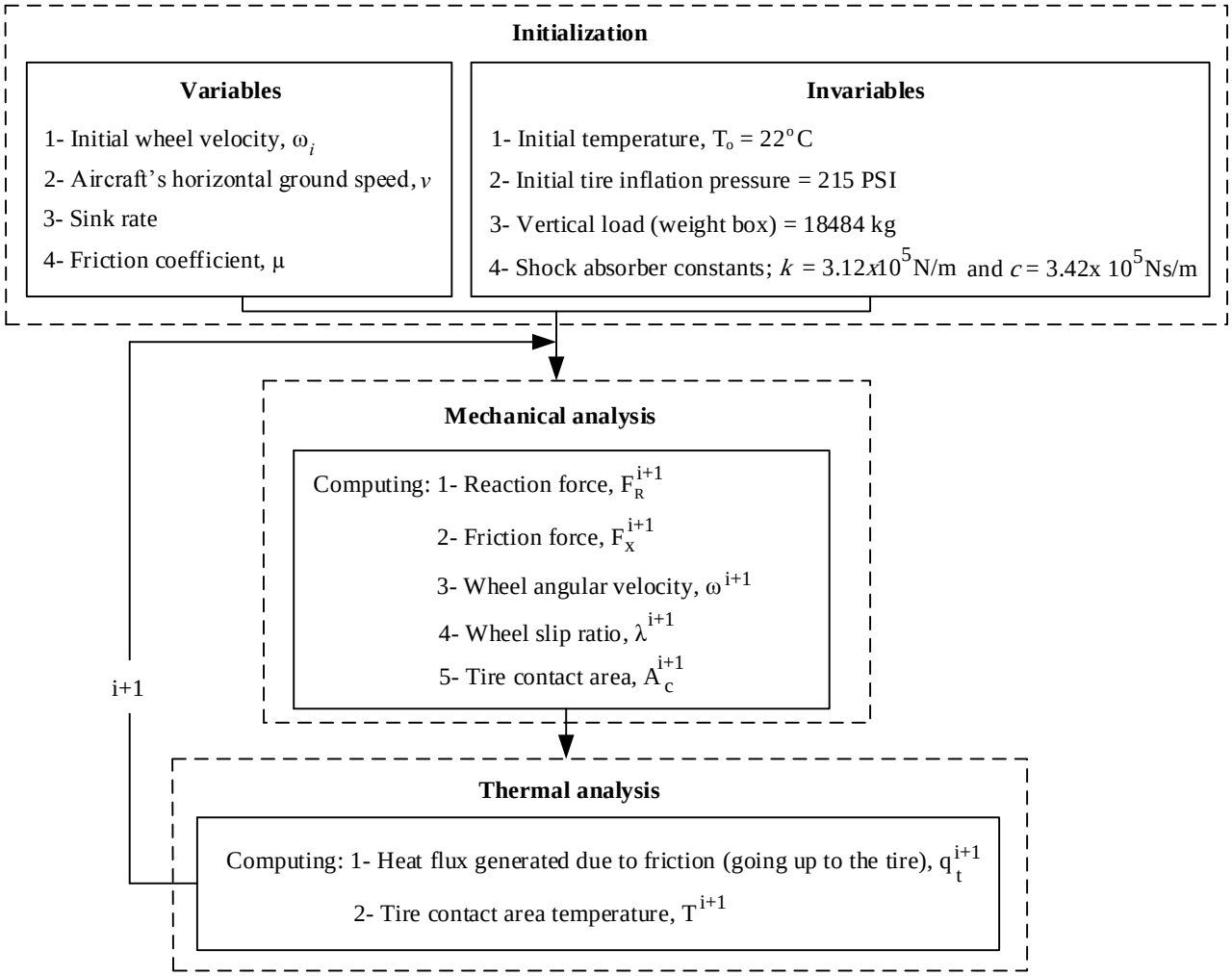

Fig. 22 Simulation process for every iteration.

The second step is the thermal analysis; where the total heat generated between the tire and runway and then the amount of heat that is going up to the tire is calculated. Finally, the tire tread contact temperature is calculated, and the process repeated many times to reach convergence.

Figure 23 shows the outline of the simulation model with some comments. The outline shows the main three sections; geometry, transient and solution. Here, the most important procedures are explained.

In the geometry section, the element 'solid226' has been used for the tire and runway to allow coupling structural-thermal analysis, as only certain combinations of elements can be used in ANSYS. The analysis has been done by using APDL (ANSYS Parametric Design Language) commands. ANSYS provides many codes (APDL) for different purposes with the option of changing the command by editing the code if required.

In the contact region between the tire and runway, the friction coefficient is applied and also there are two commands; one for calculating the total heat generated due to friction (Eq. 15) and the other command is to control the amount of heat that is going up to the tire, which is the partition coefficient (Eq. 16).

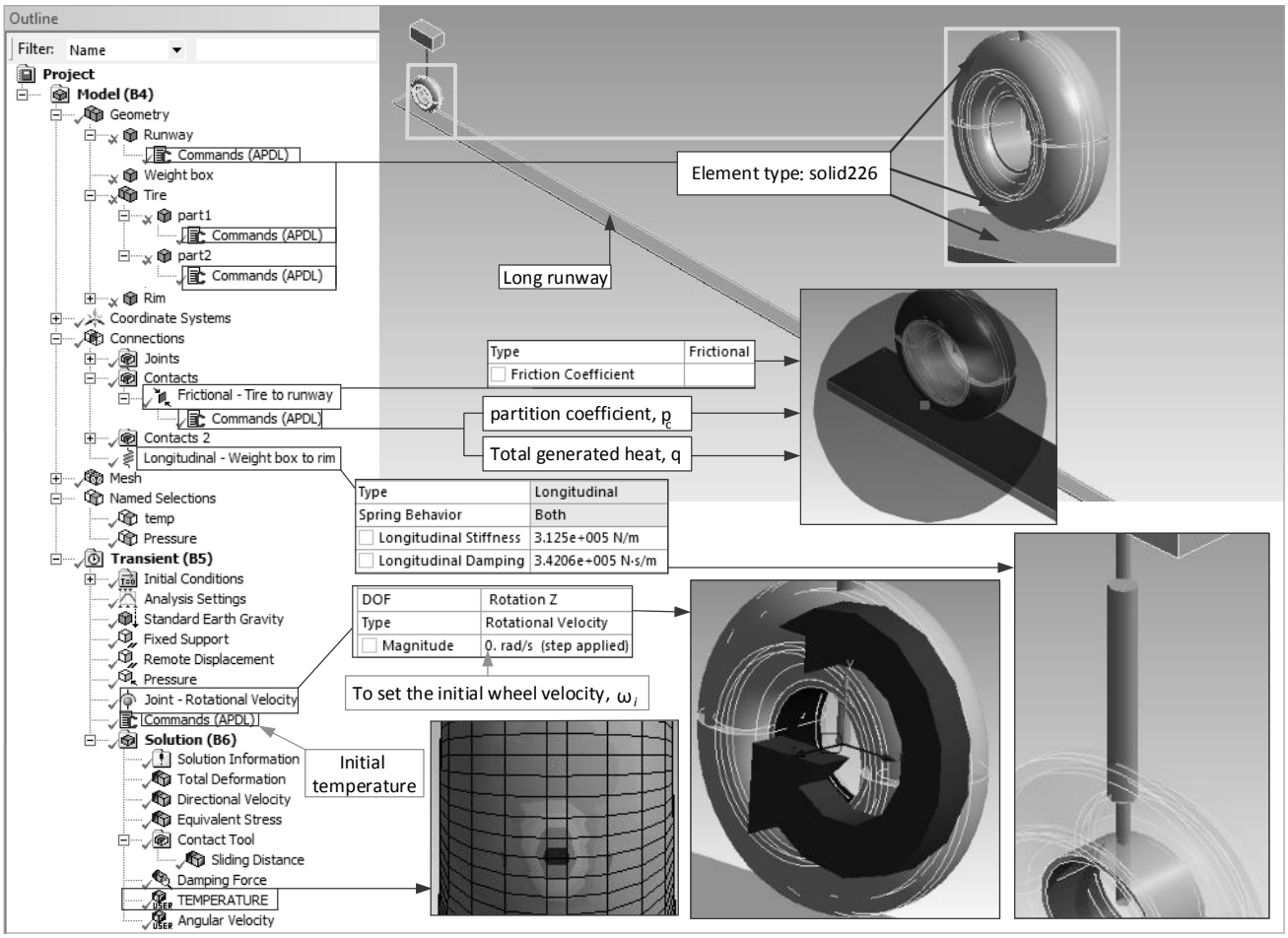

Fig. 23 Outline of the simulation model.

In the transient section, the initial conditions (horizontal speed and sink rate), analysis setting (controls of step, solver, nonlinear, and damping plus analysis data management) and the initial wheel velocity (direct input shown as 'joint-rotational velocity') are all shown. The temperature is set at 22^oC for all the simulations as an APDL command.

In the solution section, we can find all required results. For example, by using the user defined result 'TEMP' with the chosen tire tread surface, the solver will calculate the tire tread temperature. The same procedure is used to calculate the wheel angular velocity around a z axis; by using the user defined result 'OMGZ' for the wheel geometry.

References

[1] J. PADOVAN, A. KAZEMPOUR, and Y. H. KIM, "Aircraft Landing-Induced Tire Spinup", Journal of Aircraft, Vol. 28, No. 12, 1991, pp. 849–854. doi:10.2514/3.46108.

[2] E. A. Saibel and C. Tsai, "Tire Wear by Ablation" Wear, Vol. 24, No. 2, 1973, pp. 161–176. doi:10.1016/0043-1648(73)90229-9.

[3] McCarty, J. L., "Wear and related characteristics of an aircraft tire during braking" NASA, TN D-6963, 1972.

[4] Hunter, J. R., "Simple Things Won't Save The Earth", 1st ed., *University of Texas Press*, Texas , 1997, pp.1.

[5] H. Sakai and K. Araki, "Thermal Engineering Analysis of Rubber Vulcanization and Tread Temperatures During Severe Sliding of a Tire" Tire Science and Technology Vol. 27, No. 1, 1999, pp. 22–47. doi:10.2346/1.2135973.

[6] M. Bennett et al., "Composition of Smoke Generated by Landing Aircraft", Environ. Sci. Technol., Vol. 45, No. 8, 2011, pp. 3533–3538. doi:10.1021/es1027585.

[7] D. F. Hays and A. L. Browne, (Eds.), "The Physics of Tire Traction", Springer Science + Business Media, New York, 1974, pp.162-163.

[8] M. Tooley et al., "Aerospace Engineering e-Mega Reference", 1st ed., *Elsevier: Butterworth-Heinemann*, 2009, pp.133.

[9] Beazley, R. H.. U.S. Patent Application for a " Aircraft wheel spinner and control", Publication No. US2414849 A. Washington, DC: U.S. Patent and Trademark Office. 28 Jan 1947.

[10] A. Alroqi and W. Wang, "Comparison of Aircraft Tire Wear with Initial Wheel Rotational Speed", International Journal of Aviation, Aeronautics, and Aerospace, Vol. 2, No. 1, 2015, doi:10.15394/ijaaa.2015.1043.

[11] B. N. J. Persson, "Rubber Friction: Role of the Flash Temperature", J. Phys.: Condens. Matter, Vol. 18, No. 32, 2006, pp. 7789–7823. doi:10.1088/0953-8984/18/32/025.

[12] Besselink, I.J.M., "Shimmy of aircraft main landing gears", PhD dissertation, Technische Universiteit Delft, Delft, 2000.

[13] P. D. Khapane, "Gear Walk Instability Studies Using Flexible Multibody Dynamics Simulation Methods in SIMPACK" Aerospace Science and Technology, Vol. 10, No. 1, 2006, pp. 19–25. doi:10.1016/j.ast.2005.07.009.

[14] J. Padovan and P. Padovan, "Modelling Wear at Intermittently Slipping High Speed Interfaces", Computers & Structures, Vol. 52, No. 4, 1994, pp. 795–812. doi:10.1016/0045-7949(94)90361-1.

[15] T. Linke et al., "Experimental Friction and Temperature Investigation on Aircraft Tires", Tire Science and Technology, 2014, Vol. 42, No. 3, pp. 116-144.

[16] A. Kondé et al.,"Thermomechanical Analysis of an Aircraft Tire in Cornering Using Coupled Ale and Lagrangian Formulations", Open Engineering, Vol. 3, No. 2, 2013, doi:10.2478/s13531-012-0049-6.

[17] J. C. Houbolt and S. Batterson, "Some landing studies pertinent to glider-reentry vehicles", NASA technical note D-448, 1960.

[18] S. K. Clark, G. H. Nybakken, and R. J. Staples, "Laboratory Experiments on Reverted Rubber Friction", NASA CR-1398, 1969.

[19] United States Air Force," Republic F-84 Thunderjet pilot's flight operating manual", *Periscope Film*, Los Angeles, 2007, chap.7, pp. 11.

[20] Jingzhe, J., "A mixed mode function – Boundary element method for very large floating structure – Water interaction systems excited by airplane landing impacts", PhD dissertation, Southampton University, Southampton, 2007.

[21] N. E. Daidzic and J. Shrestha, "Airplane Landing Performance on Contaminated Runways in Adverse Conditions", Journal of Aircraft, Vol. 45, No. 6, 2008, pp. 2131–2144. doi:10.2514/1.38056.

[22] A. W. Mair, and D. L. Birdsall, "Aircraft performance", *Cambridge Aerospace Series 5*, 1st ed., Cambridge University Press, UK, 1992, pp.147.

[23] Ochi, Y., and K. Kanai, "Automatic Approach and Landing for Propulsion Controlled Aircraft by H/sub ∞/ Control", Proceedings of the 1999 IEEE International Conference on Control Applications, Cat. No.99CH36328, 1999, doi:10.1109/cca.1999.800951.

[24] F. Li and Z. Jiao, "Robust Control for Aircraft Anti-Skid Braking System Based on Dynamic Tire/road Friction Force Model." Proceedings of the 2nd International Conference on Computer Science and Electronics Engineering, ICCSEE 2013, doi:10.2991/iccsee.2013.409.

[25] Boeing Commercial Airplane Co., "Approach speeds for Boeing airplanes", 2011, [online database], URL: http://www.boeing.com/assets/pdf/commercial/airports/faqs/arcandapproachspeeds.pdf [cited 21 March 2015].

[26] R. Lernbeiss, "Simulation of the dynamic behavior of an aircraft landing gear during landing", Simpack User Meeting, Vienna University of Technology, 2004, URL: http://www.simpack.com/fileadmin/simpack/doc/usermeeting04/um04_tu-wien-lernb.pdf [cited 3 April 2015].

[27] Tanyolaç T., and Yasarcan H., "A soft landing model and a mass spring damper based control heuristic", Proceedings of The 29th International System Dynamics Conference, Washington, DC. 2011, URL: http://www.systemdynamics.org/conferences/2011/proceed/papers/P1119.pdf [cited 17 April 2015].

[28] A. Sinha, "Vibration of Mechanical Systems", 1st ed., *Cambridge University Press*, Cambridge, MA, 2010, pp. 25-39.

[29] A. Rao, "Realistic Simulation of a Flexible Mechanism using ANSYS Solutions", *NAFEMS World Congress*, Vancouver, Canada, May 22nd- 25th, 2007, URL: http://www.nafems.org/events/congress/2007/vendor/ [cited 21 April 2015].

[30] R. H. Daugherty, "A study of the mechanical properties of modern radial aircraft tires", NASA TM-212415, 2003.

[31] S. L. Lawrence, "Physics for scientists and engineers", 1st ed., Jones *and Bartlett Publishers*, 1996, pp.272-299.

[32] H. Tomita, "Tire-Pavement Friction Coefficient", Technical Report, Naval Civil Engineering Lab Port Hueneme, California, 1970.

[33] Y. Qiu, X. Liang, and Z. Dai, "Back stepping Dynamic Surface Control for an Anti-Skid Braking System", Control Engineering Practice, Vol. 42, Sep. 2015, pp. 140–152, doi:10.1016/j.conengprac.2015.05.013.

[34] F. Farroni et al., "TRT: Thermo Racing Tyre a Physical Model to Predict the Tyre Temperature Distribution" Meccanica, Vol. 49, No. 3, 2013, pp. 707–723, doi:10.1007/s11012-013-9821-9.

[35] Boeing Commercial Airplane Co., “Calculating Tire Contact Area”, [online database], URL: http://www.boeing.com/assets/pdf/commercial/airports/faqs/calctirecontactarea.pdf [cited 17 Dec 2015].

[36] Lufthansa Technik., “Aircraft tires: more than just rubber on steel”, [online database], URL: http://www.lufthansa-technik.com/aircraft-tires [cited 23 Dec 2015].

[37] Goodyear Co., “Aircraft data tire book”, The Goodyear Tire & Rubber Co., Akron, 2002, pp. 11,33.